



Article

Structural Pounding Effect on the Seismic Performance of a Multistorey Reinforced Concrete Frame Structure

Kosmas E. Bantilas ¹, Maria C. Naoum ¹, Ioannis E. Kavvadias ¹, Chris G. Karayannis ²
and Anaxagoras Elenas ^{1,*}

¹ Civil Engineering Department, Democritus University of Thrace, 67100 Xanthi, Greece; kbantila@civil.duth.gr (K.E.B.); mnaoum@civil.duth.gr (M.C.N.); ikavvadi@civil.duth.gr (I.E.K.)

² Civil Engineering Department, Aristotle University of Thessaloniki, 54124 Thessaloniki, Greece; karayannis@civil.auth.gr

* Correspondence: elenas@civil.duth.gr

Abstract: During intense ground motion excitations, the pounding between adjacent buildings may result in extensive structural damage. Despite the provision of regulations regarding the minimum separation gap required to prevent structural collisions, the majority of existing structures are poorly separated. The modern seismic design and assessment of structures are based on the definition of acceptable response levels in relation to the intensity of seismic action, which is usually determined by an acceptable probability of exceedance. From this point of view, the seismic performance of a typical eight-storey reinforced concrete (RC) frame structure is evaluated in terms of pounding. In particular, the performance is evaluated using six different separation gap distances as a fraction of the EC8 minimum distance. As the height of the adjacent structure affected the required separation distance, the examined RC structure was assumed to interact with four idealized rigid structures of one to four storeys. The typical storey height was equal between the examined structures; therefore, collision could occur at the diaphragm level. To this end, incidental dynamic analyses (IDAs) were performed, and the fragility curves for different limit states were obtained for each case. Finally, the seismic fragility was combined with the hazard data to evaluate the seismic performance probabilistically.

Keywords: structural pounding; reinforced concrete; performance assessment; earthquake engineering



Citation: Bantilas, K.E.; Naoum, M.C.; Kavvadias, I.E.; Karayannis, C.G.; Elenas, A. Structural Pounding Effect on the Seismic Performance of a Multistorey Reinforced Concrete Frame Structure. *Infrastructures* **2023**, *8*, 122. <https://doi.org/10.3390/infrastructures8080122>

Academic Editor: Denise-Penelope N. Kontoni

Received: 30 June 2023

Revised: 27 July 2023

Accepted: 28 July 2023

Published: 2 August 2023



Copyright: © 2023 by the authors. Licensee MDPI, Basel, Switzerland. This article is an open access article distributed under the terms and conditions of the Creative Commons Attribution (CC BY) license (<https://creativecommons.org/licenses/by/4.0/>).

1. Introduction

In the continuous building systems that are usually applied in urban areas, especially in the centres of cities, structures are built in contact with or close to each other, with small distances between them. Therefore, building structures may experience collisions or contact with adjacent structural elements when subjected to seismic excitations or other dynamic loads. Structural impact can occur at various locations throughout the structural system, including columns, beams, and floors. This phenomenon, known as pounding, poses significant challenges to the seismic design or assessment of reinforced concrete (RC) frame structures.

It is evident that the pounding between RC frame structures can harm their overall performance, ranging from localized damage to potential structural failure. Therefore, engineers and researchers must understand the mechanics of pounding, evaluate its potential consequences, and develop effective mitigation strategies to enhance the seismic resilience of RC frame structures. From the findings of field observations following numerous devastating earthquakes worldwide, it can be deduced that pounding is common when strong seismic events affect large cities and densely populated urban areas [1–4].

Modern building codes commonly include provisions for competent separation between structures to prevent pounding effects during seismic excitations [5]. However,

certain inherent factors can hinder the effectiveness and applicability of these code provisions. The fundamental principle underlying contemporary seismic codes is the recognition that intense seismic excitations can induce inelastic responses, resulting in substantial deformation. Consequently, seismic joint widths designed according to the regulations may occasionally lead to inadequate and inconsistent building separation due to the extremely nonlinear dynamic response [6,7]. Moreover, the high cost of land in city centres and the limited sizes of lots pose additional challenges to the implementation of building-separation requirements, making them less straightforward to apply. From this point of view, the minimum required separation distance between adjacent structures remains an open issue [8,9].

Over the past three decades, a considerable focus has been placed on the issue of earthquake-induced pounding between nearby buildings [10–14]. Miari et al. [15] thoroughly investigated the parameters that affect the seismic pounding between adjacent buildings. Moreover, numerous studies have examined the effects of dynamic properties and ground motion characteristics on the responses of adjacent buildings during pounding [10,16–19]. These investigations revealed that pounding becomes more pronounced when there is a significant disparity between the masses, periods, or heights of the structures involved.

While most studies have focused on buildings with equal storey heights, leading to diaphragm-to-diaphragm pounding, it is crucial to highlight that adjacent buildings exhibit varying storey heights, leading to diaphragm-to-column pounding in various cases. This type of pounding can substantially affect critical columns' responses, particularly regarding shear demand and ductility requirements [13,20,21]. Furthermore, a recent study showed the significant influence of infill panels, as these can significantly affect the responses of structures subjected to pounding during earthquakes [22]. Notably, this study specifically investigates the influence of pilotis configuration on the structural response compared to that of fully infilled frames. It also examines the effects of seismic excitation directionality on the structural response, particularly the shear behaviour of columns that suffer from collisions. Additionally, torsional pounding may occur between asymmetrically contacted adjacent buildings. Torsional pounding can substantially influence the collision of structures, resulting in increased collisions, building displacement, shear demand, torsion demand, and ductility demand [23–26].

Pounding between flexible and stiff structures has attracted the attention of several studies. However, the studies addressing this topic have yielded contradictory results. Some studies indicated that pounding amplifies the overall responses of flexible buildings while having an insignificant effect on the responses of stiff structures [6,11,27,28]. By contrast, in other cases, pounding has been found to amplify stiffer structures' responses and to suppress flexible structures' responses [29,30].

Clearly, in the presence of severe ground motion excitation, the interactions between adjacent structures can result in substantial damage. Despite the systematic research on global and local pounding-induced seismic demands, the studies related to the effects of pounding on seismic performance are limited [31]. Considering the inherent probabilistic characteristics of earthquake excitation and the record-to-record variability in the dynamic responses of structures, even when subjected to ground motions of identical intensity levels, the effect of pounding on seismic performance should be examined within a probabilistic framework. From this point of view, the seismic performance of a typical eight-storey reinforced concrete (RC) frame structure was evaluated in terms of pounding. In particular, the performance was evaluated assuming six different separation gap distances as a fraction of the Eurocode 8 (EC8) minimum distance. As the height of the adjacent structure affects the required separation distance, the examined RC structure is assumed to interact with four idealized rigid structures of one to four storeys. The typical storey height is equal between the examined structures, and collision may occur at the diaphragm level. For the scope of this study, Incidental Dynamic Analyses (IDA) [32] were performed, and fragility curves for different limit were obtained for each case. Finally, the seismic fragility was combined with hazard data to evaluate the seismic performance probabilistically.

2. Methods

2.1. Examined Cases and Numerical Modelling

The present study focuses on the seismic risk assessment of an eight-storey RC frame structure (Structure A) interacting with an adjacent low-rise rigid structure (Structure B). Since the two adjacent structures have the same storey heights, collisions may occur between the storey diaphragms and subsequently between the storey masses, resulting in floor-to-floor interaction. The investigation includes four pounding cases where the eight-storey RC frame structure interacts with adjacent rigid structures whose number of storeys ranges from one to four to examine the influence of the total height of Structure B on the pounding effect on Structure A. The examined interaction configurations between structures A and B are illustrated in Figure 1.

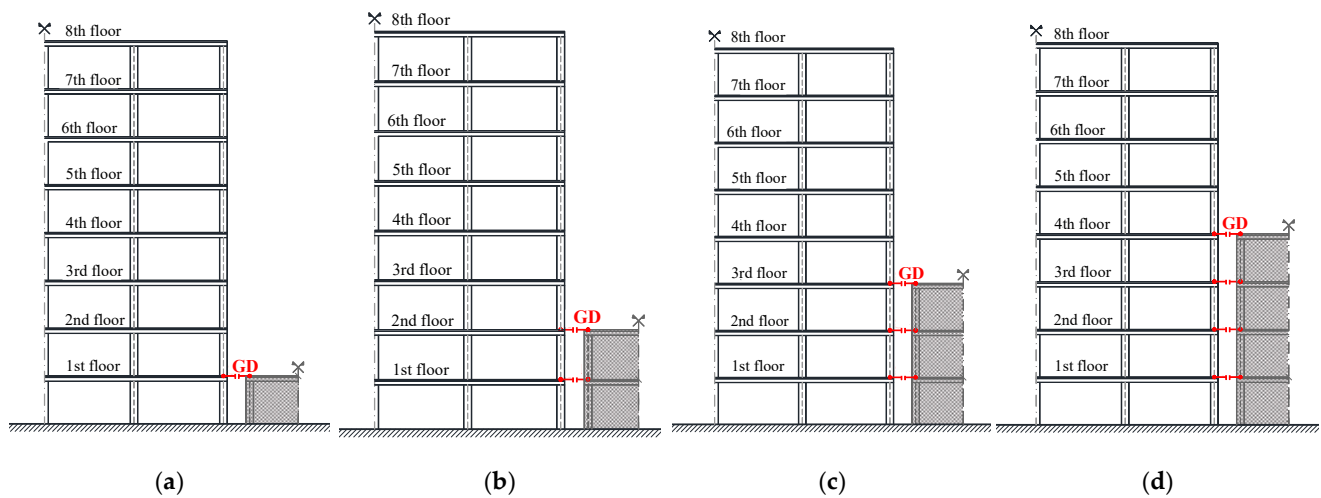


Figure 1. Schematic representation of the 8-storey RC frame that suffers interaction with a rigid structure of (a) 1 storey, (b) 2 storeys, (c) 3 storeys and (d) 4 storeys.

Among the parameters that affect pounding, the separation gap distance between the two structures is considered a major important factor. According to EC8, the minimum separation gap distance (GD) is given by the expression:

$$\Delta_{\max} = q_d \cdot d_e \tag{1}$$

where q_d is the behaviour factor, and d_e is the maximum displacement obtained via elastic analysis. When diaphragm-to-diaphragm collisions are expected, EC8 allows the minimum seismic joint (Δ_{\max}) reduction by a factor of 0.7, i.e., $GD = 0.7 \cdot \Delta_{\max}$.

Six different gap distances are considered to study the effect of the separation width on the seismic performance of the examined structure. At the same time, to assess the EC8 limitations, fractions of the provision’s compliant GD are examined. These include GDs equal to (a) Δ_{\max} , (b) $0.7 \Delta_{\max}$, (c) $0.75 \times 0.7 \Delta_{\max}$, (d) $0.50 \times 0.7 \Delta_{\max}$ and (e) $0.25 \times 0.7 \Delta_{\max}$. In addition, the case where the structures were in contact from the beginning is also considered. For comparison purposes, the seismic performance of the eight-storey RC structure without pounding is also included in the study. The six different GD values are listed in Table 1 for any case.

Table 1. Gap distances.

	In Contact	$\frac{1}{4} \cdot 0.7 \Delta_{\max}$	$\frac{1}{2} \cdot 0.7 \Delta_{\max}$	$\frac{3}{4} \cdot 0.7 \Delta_{\max}$	$0.7 \Delta_{\max}$	Δ_{\max}
Case 1	0	0.0039	0.0079	0.0118	0.0158	0.0225
Case 2	0	0.0086	0.0172	0.0258	0.0344	0.0492
Case 3	0	0.0138	0.0276	0.0414	0.0552	0.0788
Case 4	0	0.0184	0.0369	0.0553	0.0737	0.1053

The typical frame of the examined eight-storey RC structure is illustrated in Figure 2. The frame is designed according to Eurocodes 2 [33] and 8. The structure was considered as DCM, and the design for seismic actions was performed based on the following parameters: (a) seismic zone Z II, according to the Greek national annex of EC8 ($a_{gR} = 0.24 \text{ g}$), (b) soil type B ($S = 1.2$), importance factor $\gamma_I = 1$ and behaviour factor $q = 3.90$. Furthermore, concrete C25/30 and rebars B500C were assumed regarding the material’s strength classes.



Figure 2. Examined 8-storey RC frame structure.

The numerical modelling of the examined structure was performed using one-dimensional beam-column elements. The lumped plasticity model was employed to consider the material nonlinearity, which accounts for the concentrated inelastic behaviour at the ends of the elements through zero-length "plastic hinges". More precisely, the beams’ plastic hinges were modelled without considering the interaction between axial load and moment, which sets them apart from the column elements, where the yielding moment is introduced as a function of axial load. Moreover, the impact simulation relies on zero-length spring elements. These gap elements are activated since the corresponding nodes of the adjacent structures coincide, indicating contact between them. Karayannis and Naoum [24] thoroughly describe the response exhibited by the contact element. The model idealization of the examined pounding cases is presented in Figure 1.

2.2. Seismic Performance Assessment

According to the Performance-Based Earthquake Engineering (PBEE) framework [34], the seismic design or assessment of structures is based on the definition of acceptable response levels, usually expressed by the acceptable probability of exceedance during the structure’s life. Considering that the exceedance of a response level (Limit State—LS) is a Poisson process, the probability is given by the following Equation [35]:

$$P_{LS} = 1 - e^{-\lambda_{LS} \cdot t} \tag{2}$$

where λ_{LS} is the Mean Annual Frequency (MAF) of exceedance of an LS and t is the structure’s life, typically 50 years for most building structures. The MAF of exceedance is derived from the total probability theorem as follows [36]:

$$\lambda_{LS} = \int_{IM} P_f(D > C | IM) |d\lambda_{IM}| \tag{3}$$

where $P_f(D > C | IM)$ denotes the probability of demand (D) exceeding the capacity (C) given an intensity measure (IM) level, and λ_{IM} is the MAF of exceedance of an IM level. The former is referred to as seismic fragility, derived from the fragility analysis of a structure. In contrast, the latter is called seismic hazard and is derived from probabilistic seismic hazard analysis (PSHA) at a specific site [37]. The integration of the fragility curve over the seismic hazard results in the LS’s MAF of exceedance. Then, λ_{LS} can be used to obtain the seismic risk, i.e., the probability of a structure exceeding a predefined response level at a given location (see Equation (2)).

In the context of PBEE, the structural performance is assessed regarding acceptable response levels, measured by an adequately defined engineering demand parameter (EDP). In the present study, the maximum Inter-storey Drift Ratio (IDR) is adopted as EDP, and three performance levels proposed by ATC-40 [38] are investigated. The adopted performance levels are listed in Table 2.

Table 2. Adopted performance criteria.

Limit State	Maximum IDR	Performance Level
LS I	1.0%	Immediate Occupancy
LS II	1.5%	Life Safety
LS III	2.5%	Collapse Prevention

The probabilistic distribution of the LS violation at an IM level has to be assessed to derive the seismic fragility. To this end, several methods have been proposed in the literature, such as Cloud Analysis (CA), Incremental Dynamic Analysis (IDA) and Multiple Stripes Analysis (MSA) [39]. In this study, IDA is employed due to its efficiency in requiring only a single set of ground motion records instead of the MSA. Additionally, IDA allows for the derivation of analytical fragility curves without making assumptions about the relationship between the IMs and the EDPs, as seen in the CA approach. It should be noted that IDA is a versatile and broadly applicable method that extends beyond seismic fragility analysis. It serves as an effective approach to determining a structure’s collapse capacity, comprehensively understanding its response behaviour, assessing the implications of severe ground motions, and investigating changes in structural behaviour as ground motion intensity levels increase. According to this method, multiple nonlinear dynamic analyses are performed on the structural model using a suite of ground motions, each scaled to several intensity levels to derive the full range of possible responses of the structure. A set of 100 ordinary nonpulse natural ground motions, all recorded in soil type B ($v_{s,30} = 360 \div 800$ m/s), is considered to perform the IDA, while the excitation records are scaled using the 5% damped spectral acceleration that corresponds to the fundamental vibration period ($S_a(T_1, 5\%)$) [40]. The nonlinear dynamic analyses are performed using Drain-2dx v1.10 software [41].

Provided that a single EDP is adopted to define the LSs and given the IDA curves in the EDP-IM space, there are two equivalent methods to derive the seismic fragility: the horizontal and the vertical statistics procedures [42]. In the former method, demand (D) and capacity (C) are expressed in terms of the EDP. In this case, multiple horizontal cuts, which correspond to different IM levels, are performed on the IDA curves to calculate the probability that demand (EDP) exceeds capacity (EDP_C). It has to be noticed that a single horizontal cut corresponds to the discrete fragility estimation for a given IM level. Consequently, with an increase in the number of horizontal cuts, a comprehensive empirical fragility function is acquired. Subsequently, assuming a lognormal fragility function with

median μ and dispersion β , the maximum likelihood method [35] can be used to estimate the statistical moments of the fitted analytical fragility curve on the discrete fragility points. Generally, evaluating the distribution, mean value, and/or dispersion of an EDP based on the IM becomes crucial in situations where the concern focuses on loss assessment. In such cases, horizontal statistics are considered the most appropriate [43].

On the other hand, when the focus is on fragility analysis, and the objective is to determine the levels of IMs that result in EDP equal to a specific LS's capacity, the vertical statistics format is more suitable. In the vertical statistics procedure, demand and capacity are expressed in terms of IM. To this end, a vertical cut is performed on the IDA curves, corresponding to a capacity value EDP_c of an LS. It has to be mentioned that the intersecting points between the IDA curves and the vertical cut correspond to the LS's capacity in terms of IM. Therefore, the intersection points can be used to derive the probabilistic distribution of LS capacity. It is evident that lognormal distribution can adequately describe the fragility function [34]. As such, the fragility function is derived as follows [44]:

$$P_f(D > C|IM) = P_f(IM > IM_C) = \Phi\left(\frac{\ln(IM) - \ln(\hat{\mu}_c)}{\hat{\beta}_c}\right) \tag{4}$$

$$\ln(\hat{\mu}_c) = \frac{1}{n} \cdot \sum_{i=1}^n \ln(IM_{c,i}) \tag{5}$$

$$\hat{\beta}_c = \sqrt{\frac{1}{n-1} \cdot \sum_{i=1}^n (\ln(IM_{c,i}) - \ln(\hat{\mu}_c))^2} \tag{6}$$

where $\hat{\mu}_c$ is the median seismic capacity in terms of IM and $\hat{\beta}_c$ is the corresponding standard deviation, n is the number of records used to perform IDA and $IM_{c,i}$ is the intensity level of record "i" that results in a response equal to EDP_c , i.e., the intersection points between the vertical cut and the IDA curve of record "i". The two procedures are summarized in Figure 3. Due to the simplicity of the IM-basis methodology, the vertical statistics procedure is adopted in the present study to derive the seismic fragility curves of the examined structures.

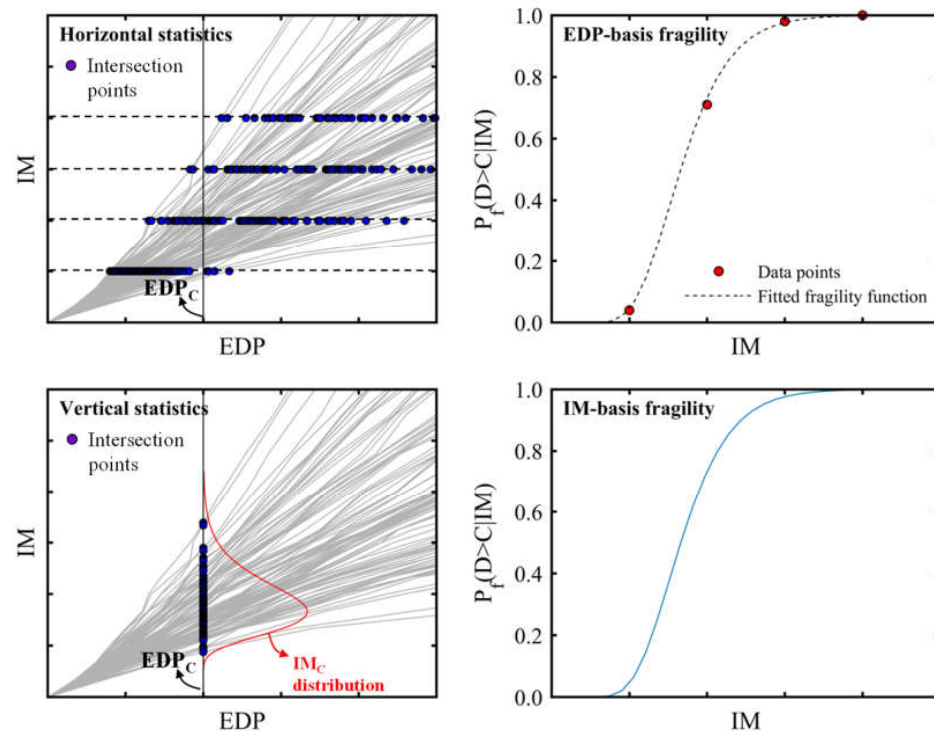


Figure 3. Comparison between EDP-basis and IM-basis methodologies to obtain fragility functions from IDA curves.

It has to be mentioned that since the LS capacity is defined deterministically only by a single value of EDP, the fragility analysis procedure presented above treats only the aleatory uncertainties, i.e., record-to-record variability. If a more precise fragility estimation is the case, then both aleatory and epistemic uncertainties must be considered by treating the LS's capacity as a random variable. A detailed review of the method can be found in [42]. As the present study focuses on the qualitative effects of pounding between adjacent structures, considering epistemic uncertainty is out of scope.

In the present study, the MAF of exceedance of an IM level is considered to follow a second-order power law as follows [45]:

$$\lambda_{IM} = k_0 \cdot \exp(-k_2 \cdot \ln^2(IM) - k_1 \cdot \ln(IM)) \tag{7}$$

where k_0 , k_1 and k_2 are constants obtained by fitting Equation (7) to the hazard data of a specific site obtained by PSHA.

Given the fragility curve of the structural model and the hazard curve at a specific site, the LS's MAF of exceedance is derived by numerical integration of Equation (3). However, in the particular case where the fragility function follows the lognormal distribution and the hazard curve follows the power law of Equation (7), the integral of Equation (3) has the following closed-form solution [45,46]:

$$\lambda_{LS} = \sqrt{p} \cdot k_0^{1-p} \cdot [\lambda_{IM}(\hat{\mu}_c)]^p \cdot \exp\left[\frac{k_1^2}{4 \cdot k_2} \cdot (1 - p)\right] \tag{8}$$

where $p = \frac{1}{1+2 \cdot k_2 \cdot \hat{\beta}_c} \exp\left[\frac{k_1^2}{4} \cdot (1 - p)\right]$.

3. Results and Discussions

3.1. Fragility Analysis

The seismic fragility must be determined to assess the seismic performance of the examined multistorey RC structure and investigate its structural pounding effect. To this end, an IDA was performed using 100 ordinary ground motion records. Specifically, an IDA was conducted on the multistorey structure, neglecting the pounding as its seismic response could be a reference measure to investigate the structural pounding effect. Subsequently, the analysis was repeated for each of the four cases regarding the height of the adjacent structure, i.e., pounding up to the first, second, third, and fourth storey, considering the six different gap distances.

The IDA curves of the examined cases are summarized in Figure 4. The figure illustrates the median curves with continuous lines, while the 16% and 84% fractiles are provided with dashed lines. It is essential to highlight that the median represents the central tendency of the IDA curves and provides an estimate of the expected response. On the other hand, the fractiles (corresponding to the ± 1 standard deviation for a lognormal distribution) represent the dispersion or variability of the response around the median. The black IDA curves correspond to the multistorey structure neglecting the pounding, while the coloured ones correspond to structural models of different gap distances. In the same figure, the LS capacity in terms of the EDP is also illustrated with dashed grey lines.

At lower intensity levels ($S_a(T_1, 5\%) < 0.1 \text{ g}$), the IDA curves are linear, and their variance remains relatively low. That fact indicates the elastic response of the examined structures without a notable pounding effect. However, as the ground motion intensity increases, the variance of the IDA curves increases, while the median maximum IDR presents a high, almost linear correlation with the IM. The former suggests the occurrence of nonlinear behaviour and potential structural damage. At the same time, the latter indicates the well-known equal displacement rule between the maximum response of a linear oscillator and an inelastic one [34]. The pounding effect results in increased seismic demands, which are more pronounced as (a) the height of the adjacent building increases, (b) the gap distance decreases, and (c) the ground motion intensity increases. In particular,

the potential pounding up to the first storey presents a minor effect on the seismic behaviour of the system. However, as the number of potential pounding locations throughout the structure’s height increases, the median IDA curves strongly deviate.

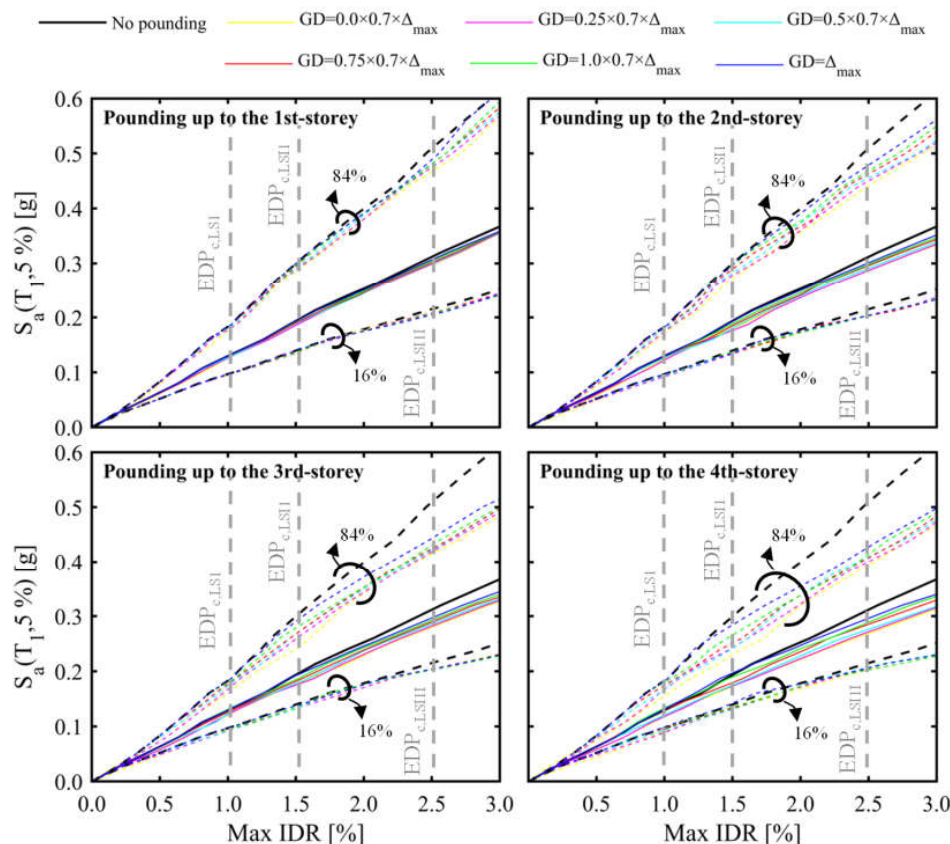


Figure 4. IDA curves of the examined cases.

Regarding the separation gap distance, if the structures are in contact, i.e., $GD = 0$ m, the collision of the adjacent structures, even at the early stages of the response, increases seismic demands. It is worth noting that increased IDR is also observed even if the separation gap equals Δ_{max} , corresponding to the structure’s maximum displacement according to EC8 provisions. Interestingly, the pounding presents a minor effect on the 16% fractile IDA curves. On the contrary, potential pounding primarily affects the median and the 84% fractile curves. As the IDA curves provide the distribution of the EDP at a given level of an IM, and vice versa, assuming a lognormal distribution of the LS capacity in terms of IM, the IDA observations indicate a reduced variation in the capacity.

To quantitatively assess the pounding effect on the dynamic response of the examined structure, the median and standard deviation of each LS capacity (in terms of IM) are presented in Figures 5 and 6, respectively. It has to be mentioned that both the median capacity ($\hat{\mu}_c$) and the standard deviation ($\hat{\beta}_c$) are normalized to the corresponding parameters of the reference model ($\hat{\mu}_{c,no\ pounding}$, $\hat{\beta}_{c,no\ pounding}$). In the absence of the pounding effect, the parameter values are provided in Table 3.

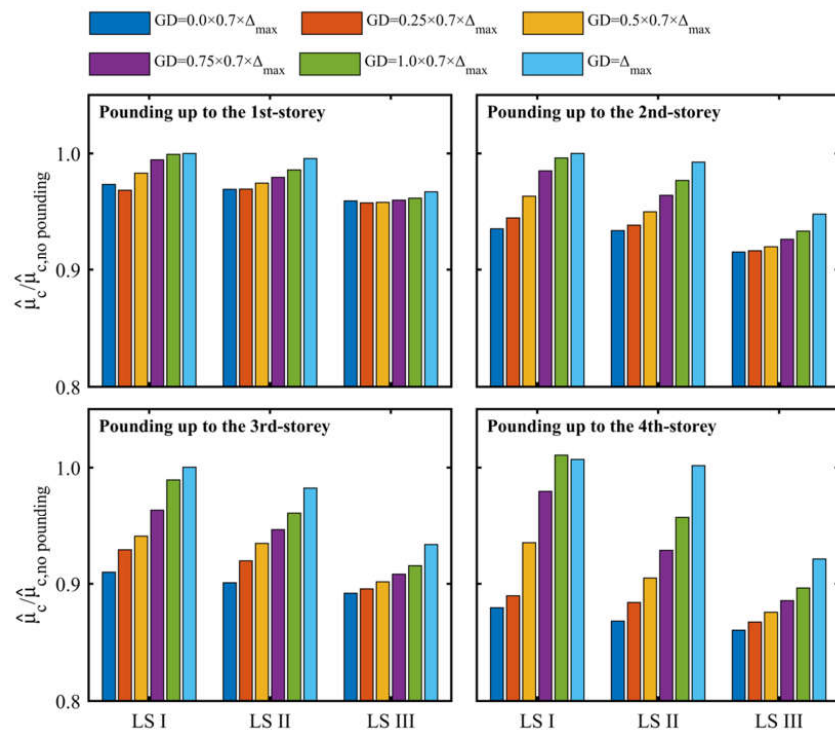


Figure 5. Comparison of the mean seismic capacity between pounding models of different gap distances and the pounding-free model.

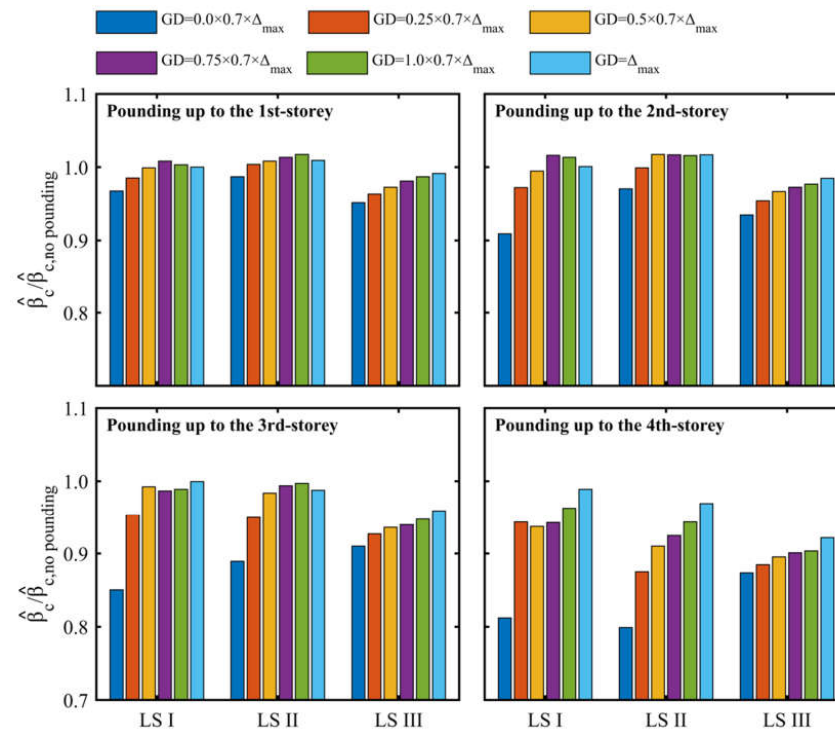


Figure 6. Comparison of the seismic capacity's standard deviation between models of different gap distances and the pounding-free structure.

Table 3. Median LS capacity and standard deviation of the multistorey structure neglecting the pounding.

Limit State	$\hat{\mu}_{c, \text{no pounding}}$	$\hat{\beta}_{c, \text{no pounding}}$
LS I	0.13 g	0.29
LS II	0.20 g	0.33
LS III	0.33 g	0.39

Concerning Figure 5, it is observed that structural pounding deteriorates the LS capacity of the examined structure, even in the case where the gap distance equals Δ_{max} . However, the pounding effect is strongly related to the height of the adjacent structure. Specifically, in the case of potential pounding between the examined multistorey frame and a single-storey adjacent rigid structure, the system presents about a 5% decrease in the LS III capacity, while in LSs I and II, the pounding effect is much less intense. In this case, the gap distance presents a minor effect on the capacity. However, as the height of the adjacent structure increases, the pounding effect tends to be pronounced, especially as the gap distance decreases. Although the pounding effect is identical on the models with seismic joint widths in compliance with EC8, in the case of pounding up to the fourth storey, the reduced gap distance ($\text{GD} = 0.7 \Delta_{\text{max}}$) results in a much higher capacity reduction in LS II. Regarding the variance of the LSs capacity, structural pounding results in decreased standard deviation values (Figure 6). Moreover, both the height of the adjacent structure and the gap distance affect the standard deviation values similar to the median capacity.

Given the median and the standard deviation of the LS capacity, Equation (4) results in seismic vulnerability. Figure 7 summarizes the seismic fragility curves of the examined models. The black curves correspond to the frame without adjacent structures, while the coloured curves correspond to the models of different gap distances. Given an IM level, the probability of exceedance of an LS increases as the gap distance decreases. This behaviour is much more pronounced as the adjacent structure’s damage state or height increases. However, as the seismic joint width increases, the fragility function tends to the vulnerability curve of the model without pounding.

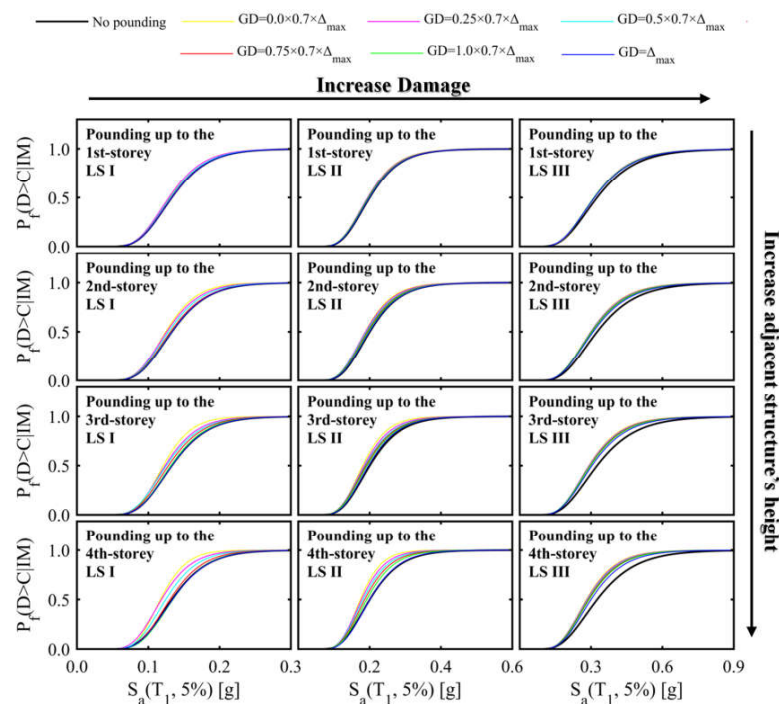


Figure 7. Seismic fragility curves of the examined structure for different limit states, gap distances and adjacent structure’s height.

3.2. Hazard Curves

Hazard curves have to be determined to investigate the pounding effect on the seismic performance of the examined structure, apart from the fragility curves of the model. In the present study, seismic hazard data that characterize the seismicity of three major cities of Greece were considered. The selected locations are categorized in the seismic zone Z II ($a_{gR} = 0.24$ g) according to the Greek national annex of EC8; therefore, the seismicity is consistent with the design assumptions of the examined structure. Moreover, these cities are characterized by densely populated centres; therefore, multistorey structures with similar characteristics to those examined could be observed.

To derive the hazard curves, spectral acceleration values, $S_a(T_1, 5\%)$, that correspond to six distinct levels of MAF of exceedance, were obtained for each location from the database of the SHARE project (Seismic Hazard Harmonization in Europe) [47]. Then, the power law of Equation (7) was fitted to the data points. The hazard curves are presented in Figure 8. The constants of the parametric hazard curves, as obtained by fitting, are also provided in the figure.

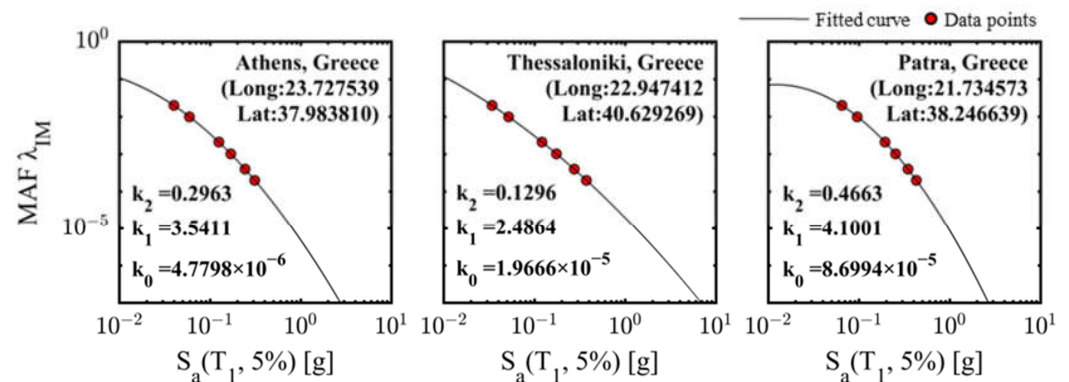


Figure 8. Seismic hazard data and fitted analytical hazard curves for the examined site locations.

3.3. Performance Assessment

The main objective of the present study is to investigate the structural pounding effect on the seismic performance of a typical multistorey RC structure under the PBEE framework. To this end, the analytical fragility functions of the examined cases and the hazard curves of the considered locations were combined to result in the LS MAF of exceedance, deploying the closed-form solution of Equation (8). Then, the probability of LS exceedance was derived by Equation (2), assuming a 50-year lifespan of the structure. The pounding effect on the seismic performance of the examined structure considering the seismic hazard of Athens, Thessaloniki, and Patra is presented in Figure 9, Figure 10, and Figure 11, respectively. The calculated probabilities were normalized to those of the reference model to highlight the pounding effect on seismic performance. The seismic performance of the reference model for the examined locations is summarized in Table 4. Comparing the probabilities of exceedance, the seismic hazard of Athens and Thessaloniki result in identical seismic performance. Even though all three locations fall within the same seismic zone, the exceedance probabilities are more than twice as high in the case of Patra. As the reference model corresponds to the multistorey structure in the absence of adjacent buildings, the normalized probabilities directly evaluate the effect of structural pounding on seismic performance.

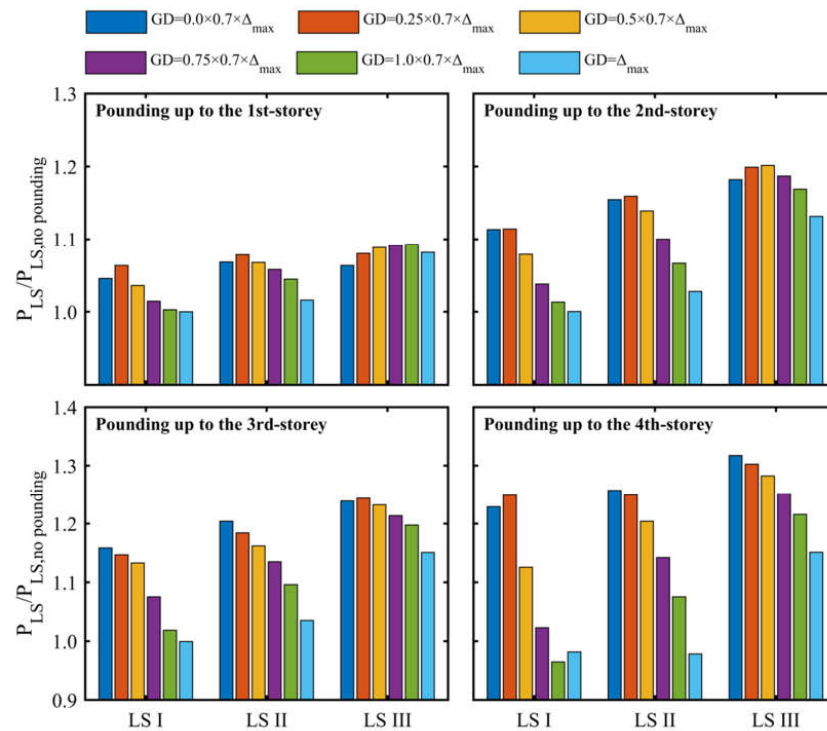


Figure 9. Pounding effect on the probability of exceedance of the examined interaction cases, considering the seismic hazard of Athens.

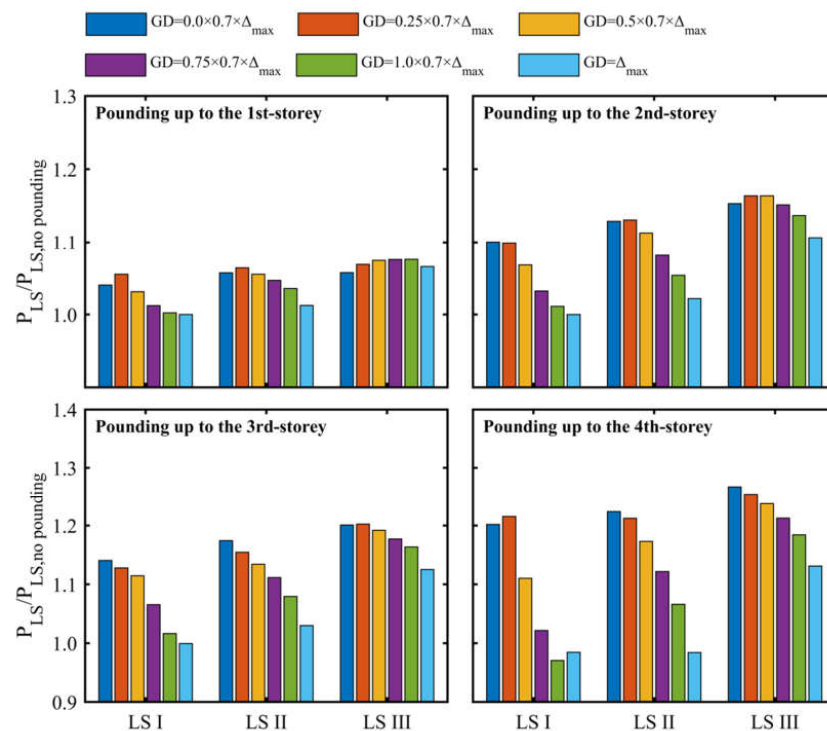


Figure 10. Pounding effect on the probability of exceedance of the LS examined interaction cases, considering the seismic hazard of Thessaloniki.

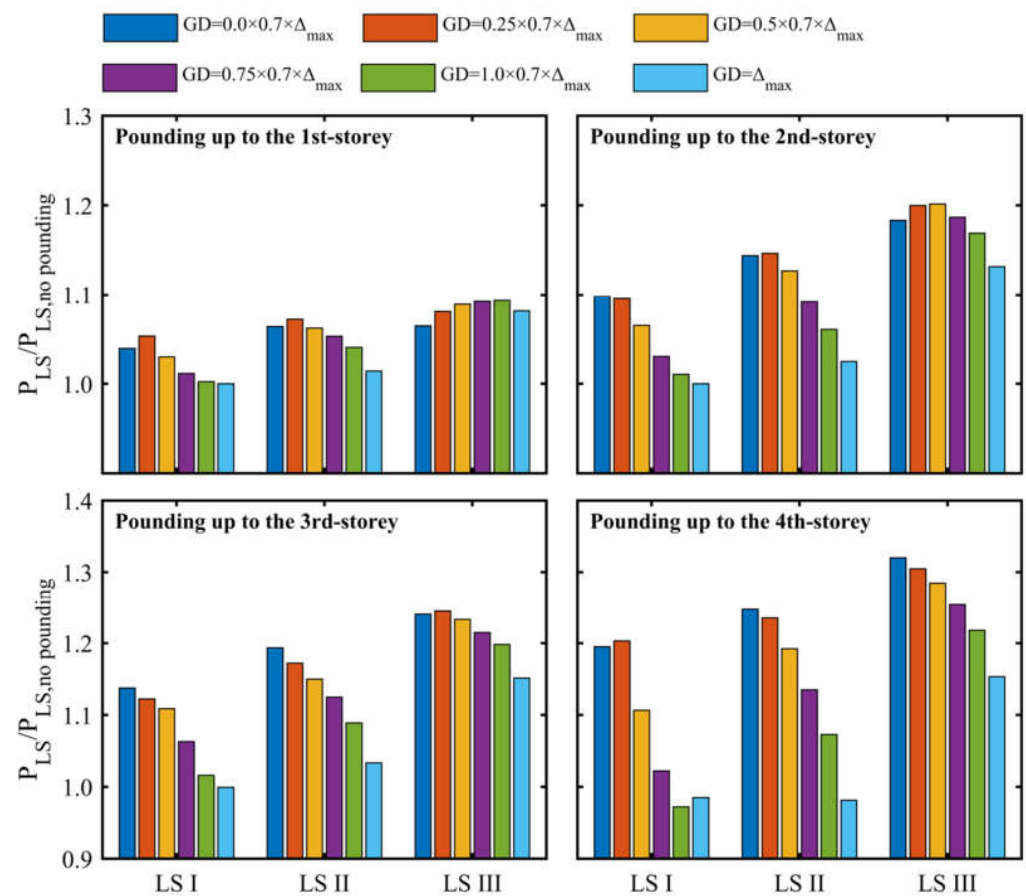


Figure 11. Pounding effect on the probability of exceedance of the examined interaction cases, considering the seismic hazard of Patra.

Table 4. LS exceedance probabilities on the examined structure in the absence of adjacent structures.

	LS I	LS II	LS III
Athens	11.0%	4.4%	1.5%
Thessaloniki	9.6%	4.6%	1.9%
Patra	25.0%	11.9%	4.1%

The parameters involved in the pounding problem, i.e., the seismic joint width and the height of the adjacent structure, seem to similarly affect the seismic performance, regardless of the seismic hazard assumption. On the other hand, the seismicity of each area significantly influences the overall performance. Among the locations under examination, it is observed that the seismic hazard associated with the city of Patra notably exacerbates the seismic performance degradation of the examined structure.

Regarding the gap distance, its effects on the seismic performance depend on both the height of the adjacent structure and the LS. The influence of the gap distance on the seismic performance is contingent upon both the height of the adjacent structure and the LS. In the case of pounding occurring up to the first storey, it is observed that a reduction in seismic joint width leads to degradation in the seismic performance within LSs I and II. This trend is reversed when considering a collapse prevention LS, as larger gap distances result in higher exceedance probabilities. However, when dealing with a single-storey adjacent structure, the probabilities of exceedance exhibit an increase of no more than 10%, signifying a minor effect of pounding in the seismic performance in such cases. The pattern mentioned above is also evident in scenarios involving two-storey adjacent structures. It is noteworthy that as the height of the adjacent structure increases, the seismic performance

further deteriorates. In the case of pounding up to the third or fourth storey, increasing the gap distance limits the pounding effect on the seismic performance.

Regarding the EC8 provisions about the minimum seismic joint width, the 30% reduced gap distance ($GD = 0.7 \Delta_{\max}$) results in slightly deteriorated seismic performance. However, the utilization of an EC8-compliant seismic joint leads to an increase in the probability of exceedance of less than 10% when considering LS I or II. Conversely, in the case of LS III, the probabilities of exceedance demonstrate an increase ranging from 10% to 20%.

4. Conclusions

The present study investigated the effect of pounding on the seismic performance of a typical eight-storey RC frame structure. As the effect of pounding depends on both the seismic joint width and the potential pounding locations throughout the structure's height, six separation gap distances and four adjacent building structures ranging from one to four storeys were examined. Considering the probabilistic characteristics of earthquake excitations and the variability in the dynamic response of a structure, the pounding effect on seismic performance was assessed in a probabilistic framework. In particular, the PBEE method was utilized to evaluate the probabilities of exceedance associated with three distinct global performance levels.

To this end, the seismic fragility of the forty-eight examined configurations (six gap distances and four adjacent structures) was evaluated. Fragility analysis revealed that the pounding effect resulted in increased seismic demands, which were more pronounced as (a) the height of the adjacent building increased, (b) the gap distance decreased, and (c) the ground motion intensity increased. Given the fragility curves, the pounding effect on the seismic performance of the examined configurations was assessed considering the seismic hazard of three major cities in Greece. The seismic hazard associated with the examined locations did not appear to exert any discernible influence on the problem parameters' effect, such as the seismic joint width and the height of the adjacent structure, on seismic performance. Moreover, structural pounding deteriorated the structure's seismic performance, even in cases where the gap distance was equal to the minimum seismic joint width proposed by EC8. In these cases, the performance deterioration ranged from about 10% to 20%, depending on the damage state of the structure.

Author Contributions: Conceptualization, K.E.B., M.C.N., I.E.K. and A.E.; methodology, K.E.B., M.C.N., I.E.K., C.G.K. and A.E.; software, K.E.B., M.C.N., I.E.K., C.G.K. and A.E.; validation, K.E.B., M.C.N. and I.E.K.; formal analysis, K.E.B., M.C.N., I.E.K., C.G.K. and A.E.; investigation, K.E.B., M.C.N., I.E.K., C.G.K. and A.E.; resources, K.E.B., M.C.N., I.E.K., C.G.K. and A.E.; data curation, K.E.B., M.C.N., I.E.K., C.G.K. and A.E.; writing—original draft preparation, K.E.B., M.C.N. and I.E.K.; writing—review and editing, C.G.K. and A.E.; visualization, K.E.B., M.C.N., I.E.K., C.G.K. and A.E.; supervision, C.G.K. and A.E.; project administration A.E. All authors have read and agreed to the published version of the manuscript.

Funding: This research received no external funding.

Data Availability Statement: The data presented in this study are available on request from the corresponding author.

Conflicts of Interest: The authors declare no conflict of interest.

References

1. Rosenblueth, E.; Meli, R. The 1985 earthquake: Causes and effects in Mexico City. *Concr. Int.* **1986**, *8*, 23–24.
2. Kasai, K.; Maison, B.F. Building pounding damage during the 1989 Loma Prieta earthquake. *Eng. Struct.* **1997**, *19*, 195–207. [[CrossRef](#)]
3. Jankowski, R. Non-linear FEM analysis of earthquake-induced structural pounding between the main building and the stairway tower of the Olive View Hospital. *Eng. Struct.* **2009**, *31*, 1851–1864. [[CrossRef](#)]
4. Cole, G.L.; Dhakal, R.P.; Turner, F.M. Building pounding damage observed in the 2011 Christchurch earthquake. *Earthq. Eng. Struct. Dyn.* **2012**, *41*, 893–913. [[CrossRef](#)]
5. *EN 1998-1*; Eurocode 8—Design of Structures for Earthquake Resistance. Part 1: General Rules, Seismic Actions and Rules for Buildings. European Committee for Standardization: Brussels, Belgium, 2004.

6. Maison, B.F.; Kasai, K. Dynamics of pounding when two buildings collide. *Earthq. Eng. Struct. Dyn.* **1992**, *21*, 771–786. [[CrossRef](#)]
7. Abdel Raheem, S.E.; Alazrak, T.; Abdel Shafy, A.; Ahmed, M.; Gamal, Y. Seismic pounding between adjacent buildings considering soil-structure interaction. *Earthq. Struct.* **2021**, *20*, 55–70.
8. Favvata, M.J. Minimum required separation gap for adjacent RC frames with potential inter-story seismic pounding. *Eng. Struct.* **2017**, *152*, 643–659. [[CrossRef](#)]
9. Liu, P.; Fan, P.P.; Zhu, H.X.; Yang, W.G. A Seismic Pounding Risk-based Method for Determination of Minimum Separation Distance between Nonlinear Adjacent Buildings. *J. Earthq. Eng.* **2022**, *26*, 7855–7877. [[CrossRef](#)]
10. Anagnostopoulos, S.A. Pounding of buildings in series during earthquakes. *Earthq. Eng. Struct. Dyn.* **1988**, *16*, 443–456. [[CrossRef](#)]
11. Jankowski, R. Assessment of damage due to earthquake-induced pounding between the main building and the stairway tower. *Key Eng. Mater.* **2007**, *347*, 339–344. [[CrossRef](#)]
12. Miari, M.; Jankowski, R. Analysis of pounding between adjacent buildings founded on different soil types. *Soil Dyn. Earthq. Eng.* **2022**, *154*, 107156. [[CrossRef](#)]
13. Karayannis, C.G.; Favvata, M.J. Inter-story pounding between multistory reinforced concrete structures. *Struct. Eng. Mech.* **2005**, *20*, 505–526. [[CrossRef](#)]
14. Jankowski, R. Pounding between inelastic three-storey buildings under seismic excitations. *Key Eng. Mater.* **2016**, *665*, 121–124. [[CrossRef](#)]
15. Miari, M.; Choong, K.K.; Jankowski, R. Seismic pounding between adjacent buildings: Identification of parameters, soil interaction issues and mitigation measures. *Soil Dyn. Earthq. Eng.* **2019**, *121*, 135–150. [[CrossRef](#)]
16. Anagnostopoulos, S.A.; Spiliopoulos, K. An investigation of earthquake induced pounding between adjacent buildings. *Earthq. Eng. Struct. Dyn.* **1992**, *21*, 289–302. [[CrossRef](#)]
17. Dimitrakopoulos, E.; Makris, N.; Kappos, A.J. Dimensional analysis of the earthquake-induced pounding between adjacent structures. *Earthq. Eng. Struct. Dyn.* **2009**, *38*, 867–886. [[CrossRef](#)]
18. Zhai, C.; Jiang, S.; Li, S.; Xie, L. Dimensional analysis of earthquake-induced pounding between adjacent inelastic MDOF buildings. *Earthq. Eng. Eng. Vib.* **2015**, *14*, 295–313. [[CrossRef](#)]
19. Mahmoud, S.; Jankowski, R. Elastic and inelastic multi-storey buildings under earthquake excitation with the effect of pounding. *J. Appl. Sci.* **2009**, *9*, 3250–3262. [[CrossRef](#)]
20. Karayannis, C.G.; Favvata, M.J. Earthquake-induced interaction between adjacent reinforced concrete structures with non-equal heights. *Earthq. Eng. Struct. Dyn.* **2005**, *34*, 1–20. [[CrossRef](#)]
21. Chenna, R.; Ramancharla, P.K. Damage assessment due to pounding between adjacent structures with equal and unequal heights. *J. Civ. Struct. Health Monit.* **2018**, *8*, 635–648. [[CrossRef](#)]
22. Manoukas, G.E.; Karayannis, C.G. Seismic Interaction between Multistory Pilotis RC Frames and Shorter Structures with Different Story Levels—Floor-to-Column Pounding. *CivilEng* **2023**, *4*, 618–637. [[CrossRef](#)]
23. Karayannis, C.G.; Naoum, M. Inter-story pounding and torsional effect due to interaction between adjacent multistory RC buildings. In Proceedings of the 6th International Conference on Computational Methods in Structural Dynamics and Earthquake Engineering COMPDYN 2017, Rhodes Island, Greece, 15–17 June 2017.
24. Karayannis, C.G.; Naoum, M.C. Torsional behavior of multistory RC frame structures due to asymmetric seismic interaction. *Eng. Struct.* **2018**, *163*, 93–111. [[CrossRef](#)]
25. Fiore, A.; Marano, G.C.; Monaco, P. Earthquake-induced lateral-torsional pounding between two equal height multi-storey buildings under multiple bi-directional ground motions. *Adv. Struct. Eng.* **2013**, *16*, 845–865. [[CrossRef](#)]
26. Wei, X.; Wang, L.; Chau, K.T. Nonlinear seismic torsional pounding between an asymmetric tower and a barrier. *Earthq. Spectra* **2009**, *25*, 899–925. [[CrossRef](#)]
27. Jankowski, R. Earthquake-induced pounding between equal height buildings with substantially different dynamic properties. *Eng. Struct.* **2008**, *30*, 2818–2829. [[CrossRef](#)]
28. Mouzakis, H.P.; Papadrakakis, M. Three dimensional nonlinear building pounding with friction during earthquakes. *J. Earthq. Eng.* **2004**, *8*, 107–132. [[CrossRef](#)]
29. Jankowski, R.; Seleemah, A.; El-Khoriby, S.; Elwardany, H. Experimental study on pounding between structures during damaging earthquakes. *Key Eng. Mater.* **2015**, *627*, 249–252. [[CrossRef](#)]
30. Gong, L.; Hao, H. Analysis of coupled lateral-torsional-pounding responses of one-storey asymmetric adjacent structures subjected to bi-directional ground motions Part I: Uniform ground motion input. *Adv. Struct. Eng.* **2005**, *8*, 463–479.
31. Flenga, M.G.; Favvata, M.J. Probabilistic seismic assessment of the pounding risk based on the local demands of a multistory RC frame structure. *Eng. Struct.* **2021**, *245*, 112789. [[CrossRef](#)]
32. Vamvatsikos, D.; Cornell, C.A. Incremental dynamic analysis. *Earthq. Eng. Struct. Dyn.* **2002**, *31*, 491–514. [[CrossRef](#)]
33. EN 1992-1-1; Eurocode 2—Design of Concrete Structures. Part 1-1: General Rules and Rules for Buildings. European Committee for Standardization: Brussels, Belgium, 2004.
34. Cornell, C.A.; Jalayer, F.; Hamburger, R.O.; Foutch, D.A. Probabilistic basis for 2000 SAC federal emergency management agency steel moment frame guidelines. *J. Struct. Eng.* **2002**, *128*, 526–533. [[CrossRef](#)]
35. Porter, K. A beginner’s guide to fragility, vulnerability, and risk. In *Encyclopedia of Earthquake Engineering*, 1st ed.; Beer, M., Kougioumtzoglou, I., Patelli, E., Au, I.K., Eds.; Springer: Berlin, Germany, 2015; pp. 235–260.

36. Günay, S.; Mosalam, K.M. PEER performance-based earthquake engineering methodology, revisited. *J. Earthq. Eng.* **2013**, *17*, 829–858. [[CrossRef](#)]
37. Kramer, S.L. *Geotechnical Earthquake Engineering*, 1st ed.; Prentice-Hall: Upper Saddle River, NJ, USA, 1996; pp. 106–138.
38. Applied Technology Council (ATC). *Seismic Evaluation and Retrofit of Concrete Buildings*; Report No. ATC-40; ATC: Redwood City, CA, USA, 1996; Volume 1.
39. Pang, Y.; Wang, X. Cloud-IDA-MSA conversion of fragility curves for efficient and high-fidelity resilience assessment. *J. Struct. Eng.* **2021**, *147*, 04021049. [[CrossRef](#)]
40. Kostinakis, K.; Fontara, I.K.; Athanatopoulou, A.M. Scalar structure-specific ground motion intensity measures for assessing the seismic performance of structures: A review. *J. Earthq. Eng.* **2018**, *22*, 630–665. [[CrossRef](#)]
41. Prakash, V.; Powell, G.H.; Campbell, S. *DRAIN-2DX Base Program Description and User's Guide, UCB/SEMM*; Report No. 17/93; University of California: Oakland, CA, USA, 1993.
42. Bakalis, K.; Vamvatsikos, D. Seismic fragility functions via nonlinear response history analysis. *J. Struct. Eng.* **2018**, *144*, 04018181. [[CrossRef](#)]
43. Mitropoulou, C.C.; Papadrakakis, M. Developing fragility curves based on neural network IDA predictions. *Eng. Struct.* **2011**, *33*, 3409–3421. [[CrossRef](#)]
44. Baker, J.W. Efficient analytical fragility function fitting using dynamic structural analysis. *Earthq. Spectra* **2015**, *31*, 579–599. [[CrossRef](#)]
45. Vamvatsikos, D. Accurate application and second-order improvement of SAC/FEMA probabilistic formats for seismic performance assessment. *J. Struct. Eng.* **2014**, *140*, 04013058. [[CrossRef](#)]
46. O'Reilly, G.J.; Yasumoto, H.; Suzuki, Y.; Calvi, G.M.; Nakashima, M. Risk-based seismic design of base-isolated structures with single surface friction sliders. *Earthq. Eng. Struct. Dyn.* **2022**, *51*, 2378–2398. [[CrossRef](#)]
47. Woessner, J.; Danciu, L.; Giardini, D.; the SHARE consortium. The 2013 European Seismic Hazard Model: Key components and results. *Bull. Earthq. Eng.* **2015**, *13*, 3553–3596. [[CrossRef](#)]

Disclaimer/Publisher's Note: The statements, opinions and data contained in all publications are solely those of the individual author(s) and contributor(s) and not of MDPI and/or the editor(s). MDPI and/or the editor(s) disclaim responsibility for any injury to people or property resulting from any ideas, methods, instructions or products referred to in the content.